

A Semi-Lagrangian Approximation of the Oren–Nayar PDE for the Orthographic Shape–from–Shading Problem

Silvia Tozza and Maurizio Falcone

Department of Mathematics, Sapienza - Università di Roma, P.le Aldo Moro 5, Rome, Italy

Keywords: Shape–from–Shading, Oren–Nayar Differential Model, Semi-Lagrangian Approximation Scheme.

Abstract: Several advances have been made in the last ten years to improve the Shape–from–Shading model in order to allow its use on real images. The classic Lambertian model, suitable to reconstruct 3D surfaces with uniform reflection properties has shown to be unsuitable for other types of surfaces, for example for rough objects consisting of materials such as clay. Other models have been proposed but it is still unclear what would be the best model. For this reason, we start our analysis for non-Lambertian surfaces. The goal being to find a unique model which should be flexible enough to deal with many kinds of real images. As a starting point for this big project, we consider the non-Lambertian Oren–Nayar reflectance model. In this paper we construct a semi-Lagrangian approximation scheme for its nonlinear partial differential equation and we compare its performances with the classical model in terms of some error indicators on series of benchmarks images.

1 INTRODUCTION

The Shape–from–Shading (SfS) problem is a classical inverse problem in Computer Vision: given a bidimensional image, the goal is to compute the three-dimensional shape of the surface from the brightness of one gray level image of that surface. The literature of this problem is huge as one see looking at the references in the survey papers (Zhang et al., 1999; Durou et al., 2008). However, the large majority of these contribution have addressed the case of Lambertian surfaces improving the model with the introduction of perspective deformations (Courteille et al., 2004; Prados et al., 2006; Breuß et al., 2012), studying several techniques to obtain a numerical approximation of the variational problem (Horn and Brooks, 1986) and of the corresponding differential model (Lions et al., 1993) or studying the corresponding photometric stereo problem (Onn and Bruckstein, 1990; Mecca and Falcone, 2013). We focus our attention on a different improvement which is intended to reduce the assumptions on the properties of the surface dealing with more general (and real) non-Lambertian surfaces. Our goal is to find a unique model which should be flexible enough to handle many different kinds of real images. To this end we want to analyze in a unified framework several models which have been proposed in the literature, e.g. (Phong, 1975; Oren and Nayar, 1995). As a starting point for

this rather big project, we consider the basic model of a single nonlinear partial differential equation (PDE) where we need to introduce new terms to tackle the general non-Lambertian case. In particular, here we consider the non-Lambertian Oren–Nayar reflectance model proposed in (Oren and Nayar, 1994; Oren and Nayar, 1995), we construct a semi-Lagrangian approximation scheme for its nonlinear PDE and we compare its performances with the classical model. Other models will be studied in a forthcoming paper (Falcone and Tozza, 2014) where we will also compare different approaches.

2 TWO SfS MODELS

In order to underline the differences, let us briefly sketch the classical Lambertian model (L–model) and the Oren–Nayar model (ON–model).

Let us consider a surface given as a graph $z = u(\mathbf{x}), \mathbf{x} \in \mathbb{R}^2$. We assume that $u(\mathbf{x}) \geq 0$ and the surface is standing on a flat background, we will denote by Ω the region inside the silhouette and we will assume (just for technical reasons) that Ω is an open and bounded subset of \mathbb{R}^2 . Moreover, we consider a single light source located at infinity. It is well known that the SfS problem is described by the image irradiance equation

$$I(\mathbf{x}) = R(\mathbf{N}(\mathbf{x})), \quad (1)$$

where $I(\mathbf{x})$ is the normalized brightness of the given grey-value image, $\mathbf{N}(\mathbf{x})$ is the unit normal to the surface at the point $(\mathbf{x}, u(\mathbf{x}))$ and $R(\mathbf{N}(\mathbf{x}))$ is the reflection map giving the value of the light reflection on the surface as a function of its orientation (i.e., of the normal) at each point. For a *Lambertian surface* the irradiance equation becomes $I(\mathbf{x}) = \gamma \mathbf{N} \cdot \omega$, where we assume to know the albedo *gamma* (in the sequel we put $\gamma = 1$ for simplicity). For Lambertian surfaces (Horn and Brooks, 1986; Horn and Brooks, 1989), just considering an orthographic projection of the scene, it is possible to model the SfS problem via a nonlinear PDE of the first order which describes the relation between the surface u (our unknown) and the brightness function I . In fact, recalling that the normal to a graph is given by $\mathbf{N}(\mathbf{x}) = (-u_{x_1}, -u_{x_2}, 1) / \sqrt{1 + |\nabla u(\mathbf{x})|^2}$, we can write (1) as

$$I(\mathbf{x}) \sqrt{1 + |\nabla u(\mathbf{x})|^2} + \tilde{\omega} \cdot \nabla u(\mathbf{x}) - \omega_3 = 0, \text{ in } \Omega \quad (2)$$

where $\tilde{\omega} = (\omega_1, \omega_2)$. This is an Hamilton-Jacobi type equation which does not admit in general regular solution. It is known that the mathematical framework to describe its weak solutions is the theory of viscosity solutions as in (Lions et al., 1993). For analytical and numerical reasons it is useful to introduce the exponential transform $\mu v(\mathbf{x}) = 1 - e^{-\mu u(\mathbf{x})}$ and change the variable. Note that here μ is a free positive parameter without a physical meaning. Following (Falcone et al., 2003), we can write (2) in a fixed point form

$$\begin{cases} \mu v(\mathbf{x}) = \min_{a \in \partial B_3} \{b(\mathbf{x}, a) \cdot \nabla v(\mathbf{x}) + f(\mathbf{x}, a, v(\mathbf{x}))\} \\ v(\mathbf{x}) = 0 \end{cases} \quad \begin{cases} \text{for } \mathbf{x} \in \Omega, \\ \text{for } \mathbf{x} \in \partial\Omega. \end{cases} \quad (3)$$

where $b(\mathbf{x}, a) = \frac{1}{\omega_3} (I(\mathbf{x})a_1 - \omega_1, I(\mathbf{x})a_2 - \omega_2)$, $f(\mathbf{x}, a, v(\mathbf{x})) = -\frac{I(\mathbf{x})a_3}{\omega_3} (1 - \mu v(\mathbf{x})) + 1$ and B_3 is the unit ball in \mathbb{R}^3 .

In contrast to the standard Lambertian case that assumes the object surface to be ideally diffusive, the *ON-model* (Oren and Nayar, 1994; Oren and Nayar, 1995) explicitly allows to handle *rough* surfaces. The idea of this model is to represent a rough surface as an aggregation of V-shaped cavities, each with Lambertian reflectance properties (see Fig. 1). The *bright-*

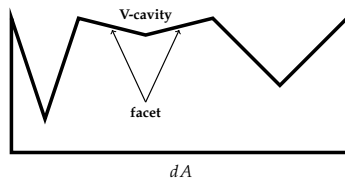


Figure 1: Facet model for surface patch dA consisting of many V-shaped Lambertian cavities.

ness equation for the ON-model is given by

$$I(\mathbf{x}) = \cos(\theta_i)A + B \sin(\alpha) \tan(\beta)M(\varphi_i, \varphi_r) \quad (4)$$

where

$$M(\varphi_i, \varphi_r) = \max[0, \cos(\varphi_i - \varphi_r)] \quad (5)$$

$$A = 1 - 0.5\sigma^2(\sigma^2 + 0.33)^{-1} \quad (6)$$

$$B = 0.45\sigma^2(\sigma^2 + 0.09)^{-1}. \quad (7)$$

Note that A and B are two nonnegative constants depending on the statistics of the cavities via the roughness parameter σ . In this model, θ_i represents the angle between the unit surface normal \mathbf{N} and the light source direction ω , θ_r stands for the angle between the unit surface normal \mathbf{N} and the camera direction \mathbf{V} , φ_i is the angle between the projection of the light source direction ω and the x_1 axis onto the (x_1, x_2) -plane, φ_r denotes the angle between the projection of the camera direction \mathbf{V} and the x_1 axis onto the (x_1, x_2) -plane (see Fig. 2), and the two variables α and β are given by

$$\alpha = \max[\theta_i, \theta_r] \text{ and } \beta = \min[\theta_i, \theta_r]. \quad (8)$$

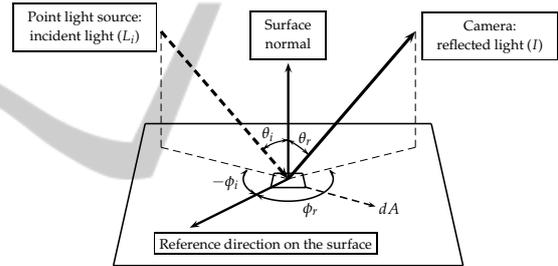


Figure 2: Diffuse reflectance for the ON-model.

For smooth surfaces, we have $\sigma = 0$ and the ON-model brings back to the L-model. To deal with this equation one has to resolve the *min* and *max* operators which appear in (4), (8). In general, some cases must be considered but here we just take one to illustrate the technique. Namely, we consider the particular case where the position of the light source ω coincides with the camera direction \mathbf{V} . This choice implies $\max[0, \cos(\varphi_i - \varphi_r)] = 1$, then defining $\theta := \theta_i = \theta_r = \alpha = \beta$, the equation (4) simplifies to

$$I(\mathbf{x}) = \cos(\theta) (A + B \sin(\theta)^2 \cos(\theta)^{-1}) \quad (9)$$

and we arrive to a Dirichlet problem for the first order nonlinear Hamilton-Jacobi equation

$$\begin{cases} (I(\mathbf{x}) - B)(\sqrt{1 + |\nabla u|^2}) + A(\tilde{\omega} \cdot \nabla u - \omega_3) \\ \quad + B \frac{(-\tilde{\omega} \cdot \nabla u + \omega_3)^2}{\sqrt{1 + |\nabla u|^2}} = 0, & \mathbf{x} \in \Omega, \\ u(\mathbf{x}) = 0 & \mathbf{x} \in \partial\Omega, \end{cases} \quad (10)$$

where $\tilde{\omega} = (\omega_1, \omega_2)$. Note that the simple homogeneous Dirichlet boundary condition is due to the

flat background behind the object but a condition like $u(x) = g(x)$ can also be considered if necessary.

Following (Falcone et al., 2003), we write the surface as $S(\mathbf{x}, z) = z - u(\mathbf{x}) = 0$, for $\mathbf{x} \in \Omega$, $z \in \mathbb{R}$, and $\nabla S(\mathbf{x}, z) = (-\nabla u(\mathbf{x}), 1)$, (10) becomes

$$\begin{cases} (I(\mathbf{x}) - B)|\nabla S(\mathbf{x}, z)| + A(-\nabla S(\mathbf{x}, z) \cdot \omega) \\ + B \left(\frac{\nabla S(\mathbf{x}, z)}{|\nabla S(\mathbf{x}, z)|} \cdot \omega \right)^2 |\nabla S(\mathbf{x}, z)| = 0, \mathbf{x} \in \Omega, \\ u(\mathbf{x}) = 0 \quad \mathbf{x} \in \partial\Omega. \end{cases} \quad (11)$$

Defining $d(\mathbf{x}, z) = \nabla S(\mathbf{x}, z)/|\nabla S(\mathbf{x}, z)|$ and $c(\mathbf{x}, z) = I(\mathbf{x}) - B + B(d(\mathbf{x}, z) \cdot \omega)^2$, using the equivalence $|\nabla S(\mathbf{x}, z)| \equiv \max_{a \in \partial B_3} \{a \cdot \nabla S(\mathbf{x}, z)\}$ we get

$$\max_{a \in \partial B_3} \{c(\mathbf{x}, z) a \cdot \nabla S(\mathbf{x}, z) - A\omega \cdot \nabla S(\mathbf{x}, z)\} = 0. \quad (12)$$

Defining the vectorfield

$$b^{ON}(\mathbf{x}, a) = \frac{1}{A\omega_3} (c_1(\mathbf{x}, z)a_1 - A\omega_1, c_2(\mathbf{x}, z)a_2 - A\omega_2) \quad (13)$$

we can finally write the nonlinear equation corresponding to the ON-model,

$$\begin{cases} \mu v(\mathbf{x}) + \max_{a \in \partial B_3} \{-b^{ON}(\mathbf{x}, a) \cdot \nabla v(\mathbf{x}) \\ + \frac{c_3(\mathbf{x}, z)a_3}{A\omega_3} (1 - \mu v(\mathbf{x}))\} = 1, \quad \mathbf{x} \in \Omega, \\ v(\mathbf{x}) = 0 \quad \mathbf{x} \in \partial\Omega. \end{cases} \quad (14)$$

3 SEMI-LAGRANGIAN APPROXIMATION SCHEMES

The numerical schemes used in this paper are based on a semi-Lagrangian approach. This method has shown to be very effective for first order problems since it tries to mimic at the discrete level the method of characteristics (see (Falcone and Ferretti, 2013) for more details). Let $W_i = w(x_i)$ so that W will be the vector solution giving the approximation of the height of u at every node x_i of the grid. The *fully discrete scheme for the classical L-model* is given by

$$W_i = T_i(W). \quad (15)$$

Denoting by P the global number of nodes in the grid, the operator $T : \mathbb{R}^P \rightarrow \mathbb{R}^P$ is defined componentwise by

$$\begin{aligned} T_i(W) = & \min_{a \in \partial B_3} \{e^{-\mu h} w(x_i + hb(x_i, a)) \\ & - \tau \frac{I(x_i)a_3}{\omega_3} (1 - \mu w(x_i))\} + \tau, \end{aligned} \quad (16)$$

where $\tau = 1 - e^{-\mu h}/\mu$ and $w(x_i + hb(x_i, a))$ is obtained interpolating on W .

It has been shown in (Falcone et al., 2003) that the

corresponding operator T has three important properties: it is monotone, is a contraction mapping in $[0, 1/\mu]^P$ and $0 \leq W \leq \frac{1}{\mu}$ implies $0 \leq T(W) \leq \frac{1}{\mu}$.

Similarly, the *SL fully discrete scheme for the ON-model* at a node x_i is given by

$$W_i = T_i^{ON}(W) \quad (17)$$

where the discrete operator T^{ON} is defined as

$$\begin{aligned} T_i^{ON}(W) = & \min_{a \in \partial B_3} \{e^{-\mu h} w(x_i + hb^{ON}(x_i, a)) \\ & - \tau \frac{c_3(x_i, z)a_3}{A\omega_3} (1 - \mu w(x_i))\} + \tau. \end{aligned} \quad (18)$$

The proof of the properties of the operator T^{ON} will appear in (Falcone and Tozza, 2014).

4 NUMERICAL TESTS

In this section we show some numerical tests to compare the two schemes described in the previous section. The algorithm for both the schemes is based on the fixed-point iteration

$$\begin{cases} V^n = T(V^{n-1}), \\ V^0 \text{ given.} \end{cases} \quad (19)$$

For the ON-model T is clearly replaced by T^{ON} .

For the synthetic images, we discretize the domain Q with 151×151 nodes. The fixed point has been computed with an accuracy of $\eta = 10^{-4}$ and the stopping rule used is $\max(|V^{n+1} - V^n|) \leq \eta$.

The first experiment is related to the paraboloid in $[-1.5, 1.5] \times [-1.5, 1.5]$ described by the function

$$z(x, y) = \begin{cases} 1 - (x^2 + y^2) & \text{if } (x^2 + y^2) < 1, \\ 0 & \text{otherwise,} \end{cases} \quad (20)$$

with light direction $\omega = (0, 0, 1)$ and visible in Fig. 3.

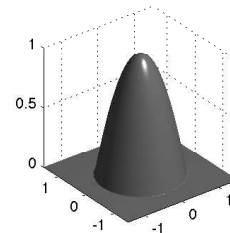


Figure 3: Test 1: Original surface $u(x, y)$.

As one can see in Fig. 4, there are no significant differences between the two surfaces reconstructed, but we can note from Tables 1, 2 and 3 that increasing of the value of the roughness parameter σ the error generated by the method of Oren-Nayar decreases

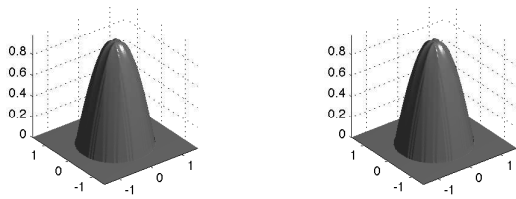


Figure 4: Test 1: Surface reconstruction, L-model (left) and ON-model with $\sigma = 0.8$ (right).

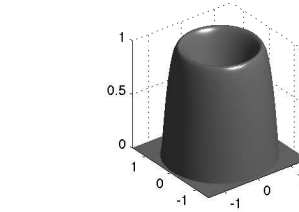


Figure 6: Test 2: Original surface $u(x,y)$.

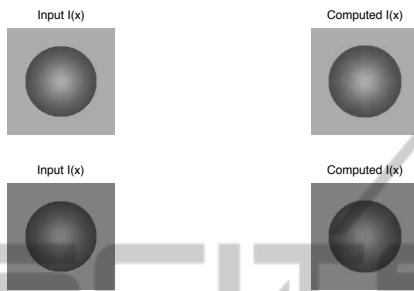


Figure 5: Test 1: Images, ON-model with $\sigma = 0.8$ (up) and L-model (down).

and it is lower than the error for the L-model. Note that for $\sigma = 0$ we get exactly the same result (since the two models coincide). In Fig. 5 the background gray level is different because it has been computed via the model.

Table 1: Test 1: L^∞ Error on the image with respect to σ .

σ	L^∞ Error Lamb	L^∞ Error ON
0	0.074826	0.074826
0.3	0.074826	0.066809
0.5	0.074826	0.058700
0.8	0.074826	0.050141
$\pi/2$	0.074826	0.041826

Table 2: Test 1: L^1 Error on the image for different values of σ .

σ	L^1 Error Lamb	L^1 Error ON
0	0.028256	0.028256
0.3	0.028256	0.025228
0.5	0.028256	0.022166
0.8	0.028256	0.018934
$\pi/2$	0.028256	0.015795

Table 3: Test 1: Standard Deviation on the image for different values of σ .

σ	Std Dev. Lamb	Std Dev. ON
0	0.007426	0.007426
0.3	0.007426	0.006631
0.5	0.007426	0.005826
0.8	0.007426	0.004976
$\pi/2$	0.007426	0.004151

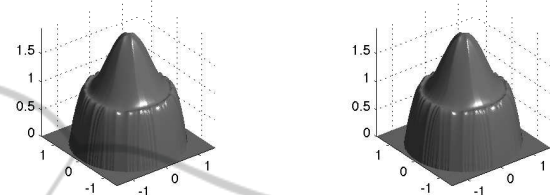


Figure 7: Test 2: Approximated surface $u(x,y)$ with the two schemes that compute the maximal viscosity solution.

The second numerical test is related to the surface described by the function

$$z(x,y) = \begin{cases} -(1 - (x^2 - y^2))^2 + 1 & \text{if } (x^2 + y^2) < 2, \\ 0 & \text{otherwise,} \end{cases} \quad (21)$$

with light direction $\omega = (0, 0, 1)$ in the same domain of the previous test (See Fig. 6 for the input surface). Looking at Fig. 7 we can note that both the schemes choose the maximal viscosity solution, which does not coincide with the original surface. In order to obtain a reconstruction closer to the original surface, we fix the value in the origin at zero. In this way we forced schemes to converge to a solution different from the maximal one (see Fig. 8). Also in this case we can see that the reconstruction of the surface is very similar with the two schemes. In Fig. 9 note that the background gray level is different for the same reason of the Fig. 5.

The next test is on a real-world image: the bust of Beethoven (see Fig. 10). The light direction is $\omega = (-0.19798, -0.01680, 0.98006)$ and the size of the input image is 77×210 . Obviously, in the case of real image, not all the values for σ are possible because the input image is given. After finding a correct value for the parameter σ , we can see again in Fig. 10 that the approximations generated by the two schemes are more or less the same, but the values in Tables 4, 5 and 6 show that the different error on the image with the ON-model are lower than the errors obtained with the L-model. Note that the improvement is more evident in Table 6.

The last test concerns the reconstruction of a vase enlightened by a vertical light source. The size of the input image is 128×128 . We can see in Fig. 11 the approximated images with the two schemes on the right,

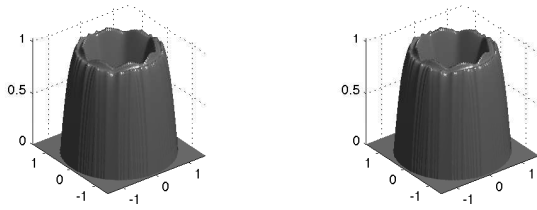


Figure 8: Test 2: Approximated surface $u(x,y)$, L-model (left) and ON-model (right).

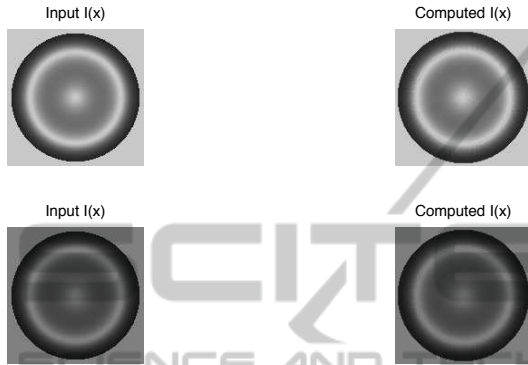


Figure 9: Test 2: Images, ON-model with $\sigma = 0.5$ (up) and L-model (down).

Table 4: L^∞ Error on the image with L-model and ON-model related to the Beethoven Test.

σ	L^∞ Error Lamb	L^∞ Error ON
0	0.635977	0.635977
0.2	0.635977	0.567406
0.4	0.635977	0.515963
0.5	0.635977	0.419684

Table 5: L^1 Error on the image with L-model and ON-model related to the Beethoven Test.

σ	L^1 Error Lamb	L^1 Error ON
0	0.047027	0.047027
0.2	0.047027	0.045838
0.4	0.047027	0.043205
0.5	0.047027	0.042169

Table 6: Standard deviation on the image with L-model and ON-model related to the Beethoven Test.

σ	Std Dev. Lamb	Std Dev. ON
0	0.056253	0.056253
0.2	0.056253	0.054361
0.4	0.056253	0.050138
0.5	0.056253	0.048308

starting from the same input image on the left. The reconstructed surface computed by both methods is shown in Fig. 12. As in the previous real test, the L^∞ and the L^1 errors obtained with the Oren-Nayar

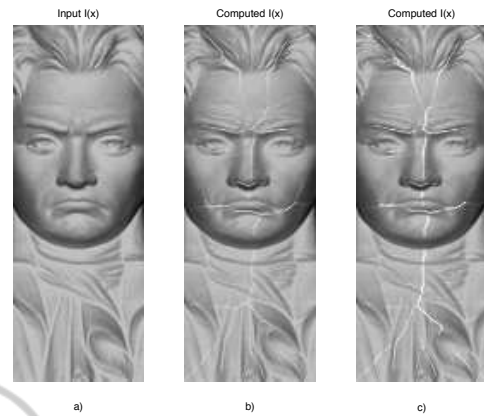


Figure 10: a) Beethoven input image. b) Oren-Nayar computed image with $\sigma = 0.4$. c) Lambertian computed image.

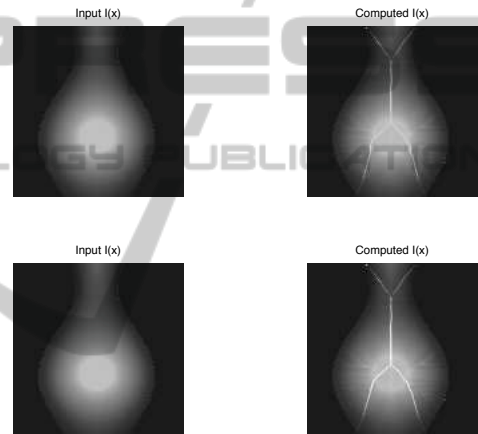


Figure 11: Vase images: ON-model with $\sigma = 0.4$ (up) and L-model (down).

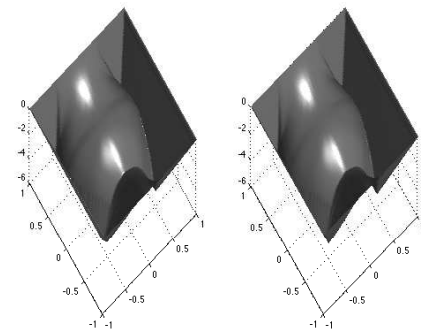


Figure 12: Vase reconstruction: L-model (left) and ON-model (right).

approach are always lower than the Lambertian errors how we can note looking at the Table 7 and 8.

Our program is to proceed in the analysis of more complex cases, e.g. synthetic images obtained with an oblique light direction, to verify that the ON-model is better than the classical L-model and to quantify

Table 7: L^∞ Error on the image with L-model and ON-model related to the vase Test.

σ	L^∞ Error Lamb	L^∞ Error ON
0	0.808202	0.808202
0.2	0.808202	0.766265
0.4	0.808202	0.678274
0.5	0.808202	0.634672

Table 8: L^1 Error on the image with L-model and ON-model related to the vase Test.

σ	L^1 Error Lamb	L^1 Error ON
0	0.028919	0.028919
0.2	0.028919	0.027292
0.4	0.028919	0.023764
0.5	0.028919	0.022190

the differences in terms of computational complexity and accuracy. We also plan to compare the results for the orthographic projection and the perspective projection model introduced in (Ju et al., 2013).

5 CONCLUSIONS

The non-Lambertian models lead to rather complex nonlinear PDEs of the first order which can be treated in the framework of weak (viscosity) solutions. The analysis of this models shows that they are not able to resolve the well known convex/concave ambiguity despite the fact that they can deal with more general surfaces. From the numerical point of view, these equations can be approximated via semi-Lagrangian techniques in a rather effective way. The role of the roughness parameter σ is crucial to obtain accurate results, playing with this parameter can in fact improve the approximation with respect to the classical L-model. In this respect, the non-Lambertian framework is more flexible and effective.

REFERENCES

- Breuß, M., Cristiani, E., Durou, J.-D., Falcone, M., and Vogel, O. (2012). Perspective shape from shading: Ambiguity analysis and numerical approximations. *SIAM J. Imaging Sciences*, 5(1):311–342.
- Courteille, F., Crouzil, A., Durou, J. D., and Gurdjos, P. (2004). Towards shape from shading under realistic photographic conditions. *17th International Conference on Pattern Recognition*, pages 277–280.
- Durou, J., Falcone, M., and Sagona, M. (2008). Numerical methods for shape from shading: a new survey with benchmarks computer vision and image understanding. *Elsevier*, 109(1):22–43.
- Falcone, M. and Ferretti, R. (2013). *Semi-Lagrangian Approximation Schemes for Linear and Hamilton-Jacobi Equations*. SIAM.
- Falcone, M., Sagona, M., and Seghini, A. (2003). A scheme for the shape-from-shading model with "black shadows". In *Numerical Mathematics and Advanced Applications*. Springer-Verlag.
- Falcone, M. and Tozza, S. (2014). Analysis and approximation of some Shape-from-Shading models for non-lambertian surfaces. *Forthcoming*.
- Horn, B. and Brooks, M. (1986). The variational approach to shape from shading. *Computer Vision, Graphics, and Image Processing*, 33(2):174–208.
- Horn, B. and Brooks, M. (1989). *Shape from Shading*. The MIT Press.
- Ju, Y. C., Tozza, S., Breuß, M., Bruhn, A., and Kleefeld, A. (2013). Generalised Perspective Shape from Shading with Oren-Nayar Reflectance. In *Proceedings of the 24th British Machine Vision Conference (BMVC 2013)*, Bristol, UK. BMVA, BMVA Press.
- Lions, P. L., Rouy, E., and Tourin, A. (1993). Shape-from-shading, viscosity solutions and edges. *Numerische Mathematik*, 64(3):323–353.
- Mecca, R. and Falcone, M. (2013). Uniqueness and approximation of a photometric shape-from-shading model. *SIAM J.*, 6(1):616–659.
- Onn, R. and Bruckstein, A. M. (1990). Integrability disambiguates surface recovery in two-image photometric stereo. *International Journal of Computer Vision*, 5(1):105–113.
- Oren, M. and Nayar, S. (1994). Generalization of Lambert's reflectance model. In *Proc. International Conference and Exhibition on Computer Graphics and Interactive Techniques (SIGGRAPH)*, pages 239–246.
- Oren, M. and Nayar, S. (1995). Generalization of the Lambertian model and implications for machine vision. *International Journal of Computer Vision*, 14(3):227–251.
- Phong, B. (1975). Illumination for computer generated pictures. *Communications of the ACM*, 18(6):311–317.
- Prados, E., Camilli, F., and Faugeras, O. (2006). A viscosity solution method for shape-from-shading without image boundary data. *ESAIM: Mathematical Modelling and Numerical Analysis*, 40(2):393–412.
- Zhang, R., Tsai, P.-S., Cryer, J., and Shah, M. (1999). Shape from shading: a survey. *IEEE Transactions on Pattern Analysis and Machine Intelligence*, 21(8):690–706.